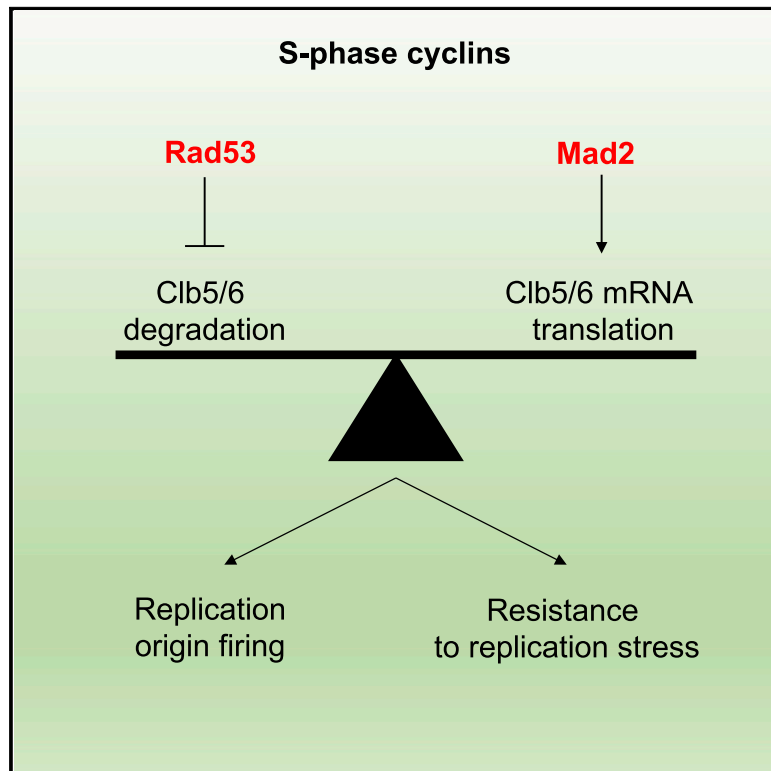


# A Mad2-Mediated Translational Regulatory Mechanism Promoting S-Phase Cyclin Synthesis Controls Origin Firing and Survival to Replication Stress

## Graphical Abstract



## Authors

Sophie Gay, Daniele Piccini, Christopher Bruhn, ..., Walter Carotenuto, Stefano Biffo, Marco Foiani

## Correspondence

sophie.gay@ifom.eu (S.G.), marco.foiani@ifom.eu (M.F.)

## In Brief

Here, Gay et al. show that, in addition to its well-established role in the spindle checkpoint, Mad2 promotes translation of S-phase cyclin mRNAs. This S-phase role of Mad2 is critical for cell survival following replication stress.

## Highlights

- Mad2 promotes origin firing in *rad53* defective cells upon replication stress
- Rad53 inhibits Clb5 degradation, while Mad2 promotes Clb5 synthesis
- Mad2 inhibits Caf20<sup>4E-BP</sup> by modulating its interaction with the translation machinery
- The role of Mad2 in translation does not depend on other SAC proteins



# A Mad2-Mediated Translational Regulatory Mechanism Promoting S-Phase Cyclin Synthesis Controls Origin Firing and Survival to Replication Stress

Sophie Gay,<sup>1,\*</sup> Daniele Piccini,<sup>1</sup> Christopher Bruhn,<sup>1</sup> Sara Ricciardi,<sup>2,3</sup> Paolo Soffientini,<sup>1</sup> Walter Carotenuto,<sup>1</sup> Stefano Biffo,<sup>2,3</sup> and Marco Foiani<sup>1,3,4,\*</sup>

<sup>1</sup>IFOM, The FIRC Institute of Molecular Oncology, Via Adamello 16, 20139 Milan, Italy

<sup>2</sup>Fondazione Istituto Nazionale Genetica Molecolare, Via Francesco Sforza, 32, 20122 Milan, Italy

<sup>3</sup>Università degli Studi di Milano, Via Celoria 26, 20133 Milan, Italy

<sup>4</sup>Lead Contact

\*Correspondence: [sophie.gay@ifom.eu](mailto:sophie.gay@ifom.eu) (S.G.), [marco.foiani@ifom.eu](mailto:marco.foiani@ifom.eu) (M.F.)

<https://doi.org/10.1016/j.molcel.2018.04.020>

## SUMMARY

Cell survival to replication stress depends on the activation of the Mec1<sup>ATR</sup>-Rad53 checkpoint response that protects the integrity of stalled forks and controls the origin firing program. Here we found that Mad2, a member of the spindle assembly checkpoint (SAC), contributes to efficient origin firing and to cell survival in response to replication stress. We show that Rad53 and Mad2 promote S-phase cyclin expression through different mechanisms: while Rad53 influences Clb5,6 degradation, Mad2 promotes their protein synthesis. We found that Mad2 co-sediments with polysomes and modulates the association of the translation inhibitor Caf20<sup>4E-BP</sup> with the translation machinery and the initiation factor eIF4E. This Mad2-dependent translational regulatory process does not depend on other SAC proteins. Altogether our observations indicate that Mad2 has an additional function outside of mitosis to control DNA synthesis and collaborates with the Mec1-Rad53 regulatory axis to allow cell survival in response to replication stress.

## INTRODUCTION

Inhibition of replication fork progression activates the Mec1<sup>ATR</sup>-mediated checkpoint that phosphorylates downstream effectors such as Rad53<sup>Chk1</sup> (Branzei and Foiani, 2009). Once activated, the replication checkpoint stabilizes stalled replication forks (Sogo et al., 2002), stimulates dNTP production (Zhao et al., 1998; Zhao and Rothstein, 2002), influences origin firing (Marheineke and Hyrien, 2004; Santocanale and Diffley, 1998), regulates histone protein levels (Gunjan and Verreault, 2003), and releases topological tensions (Bermejo et al., 2012). Later in the cell cycle, the spindle assembly checkpoint (SAC) controls the bipolar attachment of chromosomes to microtubules (Foley and Kapoor, 2013; Musacchio, 2015). Abnormal physical tension between chromosomes and microtubules is sensed at the kinetochore

by the Knl1 complex–Mis12 complex–Ndc80 complex (KMN network) (Godek et al., 2015) that recruits the mediator complex Mad1/Mad2 (Figure 1A). After activation, Mad2 forms a soluble effector complex with the proteins Bub3, Mad3<sup>BubR1</sup>, and Cdc20, which inhibits the anaphase-promoting complex (APC) (Fraschini et al., 2001; Sudakin et al., 2001). APC inhibition prevents the degradation of mitotic cyclins (Clb2<sup>CyclinB</sup>) and Pds1<sup>Securin</sup>, thus blocking the metaphase/anaphase transition (Shirayama et al., 1999; Wäsch and Cross, 2002). Deregulation of SAC protein expression causes chromosome instability and cancer (Schuyler et al., 2012; Suijkerbuijk and Kops, 2008).

Despite the persistence of Mad1 and Mad2 proteins throughout the cell cycle, their role outside of mitosis is elusive. During interphase, Mad1 and Mad2 mainly localize to nuclear pores (Campbell et al., 2001; De Souza et al., 2009; Lee et al., 2008; Lussi et al., 2010). In the yeast *Saccharomyces cerevisiae*, Mad1, but not Mad2, favors protein nuclear transport and modulates nuclear import following SAC activation (Cairo et al., 2013). Mad2 has been shown to physically interact with proteins involved in transcription, mRNA processing, and translation (Batisse et al., 2009; Graumann et al., 2004; Uetz et al., 2000; Wong et al., 2007; Yu et al., 2008), although the involvement of Mad2 in these processes is still elusive.

We found that Mad2 contributes to cell survival in response to replication stress when the Rad53 checkpoint is defective. While Rad53 influences Clb5,6 degradation, Mad2 promotes Clb5,6 protein synthesis through its association with the inhibitor of translation Caf20<sup>4E-BP</sup>. Altogether our observations indicate that Mad2, and not the other SAC proteins, counteracts the association of Caf20 with the translational machinery and stabilizes the complex formation between Caf20 and the initiation factor Cdc33<sup>eIF4E</sup>. Hence, Mad2 acts also during S-phase to promote origin firing and, together with the Rad53-mediated checkpoint, contributes to cell survival in response to replication stress.

## RESULTS

### Mad2 Contributes to Cell Survival in Response to Replication Stress when Rad53 Is Not Functional

We investigated whether spindle checkpoint proteins were required for survival to hydroxyurea (HU)-induced replication



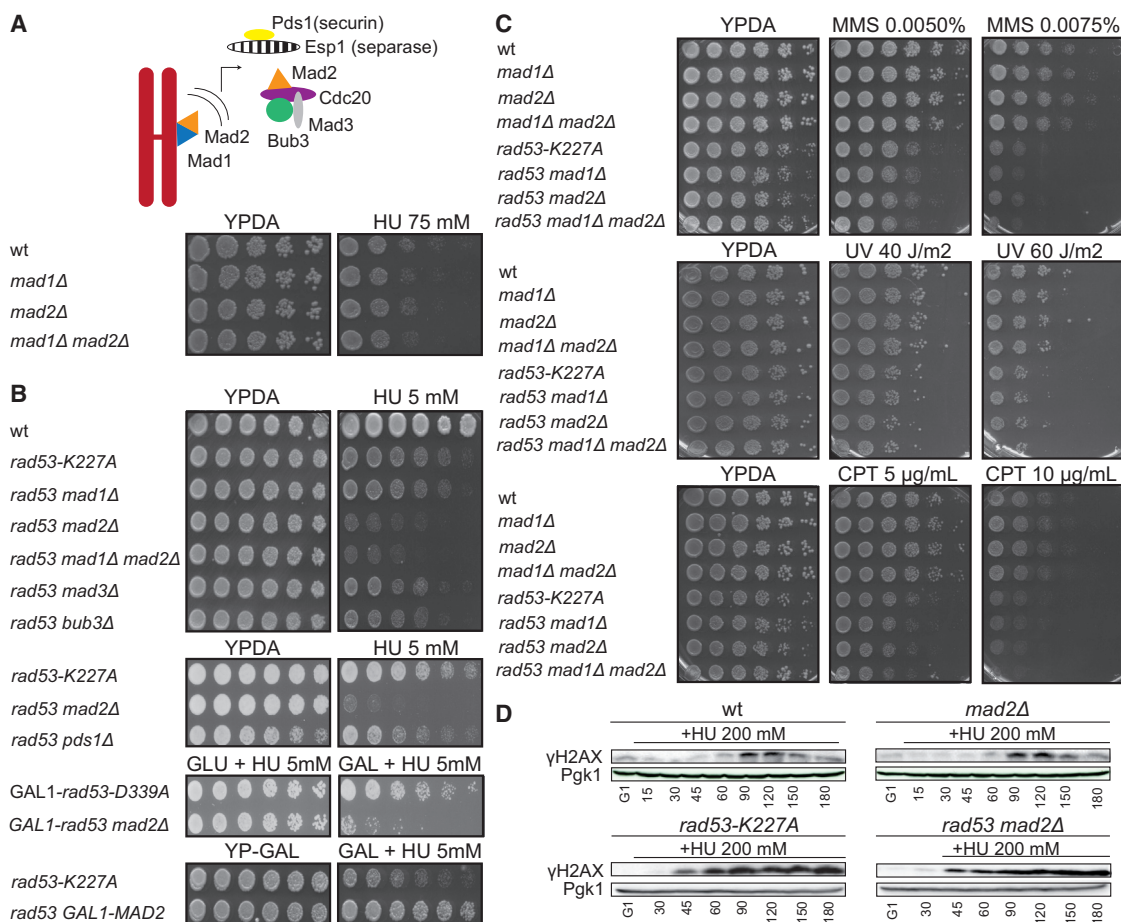


**Figure 1. MAD2 Deletion Increases the Sensitivity of *rad53* Mutants to Replication Stress**

(A) Schematic representation of the SAC activation.

(A–C) Cells were spotted in 5-fold (A and C) or 2-fold (B) serial dilutions on YPDA/YP-Gal/HU/MMS or camptothecin plates, or on plates irradiated with UV. Relative growth was assayed after 2 days of culture at 28°C. The *rad53-K227A* allele is marked as *rad53*, and the *GAL1-rad53-D339A* allele is marked as *GAL1-rad53*.

(D) DNA damage induced by replication stress was monitored by western blot analysis using anti-phosphorylated H2AX antibodies. Cells were synchronized in G1 and released into YPD + 200 mM HU. Pgk1 was used as a loading control.

stress (Krakoff et al., 1968). The HU sensitivity of *mad1Δ* and *mad2Δ* mutants was comparable to the one of isogenic wild-type (WT) cells (Figure 1A). However, when combined with the *rad53-K227A* mutation, which retains 10% of Rad53 kinase activity (Zheng et al., 1993), *mad2Δ* synergistically enhanced the HU sensitivity of *rad53-K227A*, while Mad2 overexpression ameliorated the *rad53* HU sensitivity (Figure 1B). *mad1Δ*, *mad3Δ*, and *bub3Δ* did not display any synthetic interactions with the *rad53* mutation, and the triple mutant *rad53-K227A mad1Δ mad2Δ* exhibited the same HU sensitivity of the *rad53-K227A mad2Δ* double mutant (Figure 1B). Once activated, Mad2 inhibits the APC, which degrades the securin Pds1, thus avoiding premature chromatid separation (Shirayama et al., 1999) (Figure 1A). We compared the HU sensitivity of *rad53-K227A pds1Δ* and *rad53-K227A* mutants (Figure 1B) and found that Pds1 did not contribute to the response to replication stress in a *rad53* background, thus suggesting that the enhanced HU sensitivity of *rad53-K227A mad2Δ* mutants was

not caused by premature chromatid segregation. Overexpression of the dominant-negative *rad53-K339A* allele also caused synthetic HU sensitivity when combined with *mad2Δ* (Figure 1B). We conclude that specifically Mad2, within the SAC apparatus, is required for cell survival to replication stress in a *rad53* background.

Mad2 is the only component of the spindle checkpoint containing a HORMA domain (for Hop1, Rev7, and MAD2) (Aravind and Koonin, 1998); we tested whether the enhanced HU sensitivity caused by *mad2Δ* was a common feature associated with the loss of a protein carrying such a domain. Rev7, a subunit of DNA polymerase zeta, is involved in translesion synthesis, and the HORMA domains of Rev7 and Mad2 can partially substitute for each other *in vitro* (Hanafusa et al., 2010). However, *rev7Δ* did not exhibit any synthetic defect with *rad53* in the presence of HU (Figure S1A). Moreover, *mad2Δ* did not modify the levels of Rad53 phosphorylation in response to replication stress (Figure S1B).

Rad53 mediates cell survival under replication stress conditions but also under DNA damaging conditions. We tested the effect of *MAD2* deletion in cells treated with the alkylating agent methyl methan-sulfonate (MMS); ultraviolet (UV) radiation, which leads to the formation of thymine dimers; or camptothecin (CPT), which forms a covalent complex between topoisomerase I and DNA. In all cases *rad53-K227A* mutants exhibited hypersensitivity compared to WT cells (Figure 1C); however, the combination of *MAD2* deletion with *rad53-K227A* mutation did not cause synthetic growth defects upon DNA damage (Figure 1C). These results suggest that *MAD2* deletion specifically affects the HU-induced replication stress response and not the DNA damage response of *rad53-K227A* mutants. Accordingly, the levels of H2AX phosphorylation, a readout of DNA damage, were comparable in WT and *mad2Δ* cells as well as in *rad53-K227A* and *rad53-K227A mad2Δ* mutants (Figure 1D).

### Mad2 Influences Origin Firing in Response to Replication Stress

We then investigated whether the absence of Mad2 affected replication dynamics. WT, *mad1Δ*, *mad2Δ*, and *mad1Δ mad2Δ* cells were released from G1 into 200 mM HU for 1, 2, or 3 hr and analyzed by neutral-neutral 2D gels electrophoresis after *in vivo* chromatin psoralen crosslinking (Brewer and Fangman, 1987). At 1 hr in HU, all strains accumulated, at the *ARS305* locus, bubble intermediates, a readout of origin firing, and large Y structures, indicative of an asymmetric progression of the sister forks (Figure S2A). The replication intermediates progressively diminished at 2 and 3 hr in HU as a result of fork progression outside the restriction fragment analyzed. The quality and the kinetics of appearance/disappearance of the replication intermediates were comparable in all the strains analyzed. Moreover, the levels of incorporation of bromodeoxyuridine (BrdU), a thymidine analog, analyzed at early origins (*ARS305*, *ARS306*, *ARS607*), and at the centromeric origin *ARS308*, were also comparable in WT and *mad2Δ* strains released from G1 into HU (Figures S2B and S2C). As expected, no BrdU incorporation was detected at inactive origins (Figure S2D). We conclude that the deletion of *MAD2 per se* does not influence origin firing.

We then examined by 2D gels the *ARS305* replication intermediates of *rad53-K227A*, *rad53-K227A mad1Δ*, *rad53-K227A mad2Δ*, and *rad53-K227A mad1Δ mad2Δ* strains released from G1 into HU (Figure 2A). *rad53-K227A* mutants accumulated the typical intermediates resulting from origin firing and progressive fork collapse (Lopes et al., 2001). *rad53-K227A* and *rad53-K227A mad1Δ* mutants exhibited comparable replication profiles. However, the deletion of *MAD2* in a *rad53-K227A* or *rad53-K227A mad1Δ* backgrounds caused a significant reduction (about five times) in the levels of replication intermediates, without altering their kinetics of appearance/disappearance. BrdU immunoprecipitation and quantitative PCR confirmed that the deletion of *MAD2* in *rad53-K227A* mutants reduces origin firing at early origins and extended this observation to late origins (*ARS106*) (Figures 2B and 2C). We conclude that in the absence of a functional Rad53, *MAD2* deletion leads to a decrease in origin firing efficiency.

### Mad2 and the Intra-S Checkpoint promote the Expression of the S-Phase Cyclins Clb5,6

Replication origin firing is a two-step process mediated by origin licensing and origin activation (Bell and Dutta, 2002; Diffley and Labib, 2002). During this later step, a subset of the potential origins bound by a pre-replicative complex are converted into active origins through a phosphorylation cascade which involves the DBF4-dependent kinase DBF4/Cdc7 and the cyclin-dependent kinases (CDKs) Clb5/Cdc28 and Clb6/Cdc28. *clb5Δ* cells exhibit a prolonged S-phase, a decrease in late origin firing in the absence of replication stress, and an increased sensitivity to HU (Donaldson et al., 1998; Epstein and Cross, 1992; Hsu et al., 2011). Moreover, *CLB5* deletion is lethal in combination with a defective intra-S checkpoint, suggesting that Clb5 levels become particularly critical in the absence of a functional intra-S checkpoint (Gibson et al., 2004; Manfrini et al., 2012). We investigated whether Clb5 levels were affected by *MAD2* deletion or *RAD53* mutations. WT, *mad2Δ*, *rad53-K227A*, and *rad53-K227A mad2Δ* cells were synchronized in G1 and released into S-phase. Clb5 levels were analyzed throughout the cell cycle by western blotting. As previously described (Jackson et al., 2006), Clb5 accumulation started roughly 30 min after release from G1. Its levels peaked after 60 min from release and declined when cells went through mitosis (Figures 3A and 3B). Clb5 expression profile was similar in *mad2Δ* and WT cells, even though we observed a 40% loss in Clb5 levels at 75 min from the G1 release in *mad2Δ* cells compared to WT. We note that this loss was not due to a faster S-phase since FACS profiles were comparable in WT and *mad2Δ* cells (Figure 3B). In *rad53* mutants, Clb5 accumulated with similar kinetics to WT cells. The contribution of Mad2 in the maintenance of Clb5 levels was far more evident when comparing *rad53-K227A* and *rad53-K227A mad2Δ* cells. Although the kinetics of Clb5 accumulation were similar between the two strains, Clb5 protein levels were between 30% and 60% less abundant in *rad53-K227A mad2Δ* cells compared to *rad53-K227A* cells (45–90 min after release from G1). Altogether, these results suggest that Mad2 influences the accumulation of Clb5 levels, even in the absence of replication stress.

We then studied the effect of replication stress on the Clb5 accumulation by releasing cells in complete medium in the presence of HU (Figure 3A). As previously described (Palou et al., 2010), in WT cells, Clb5 levels peaked 60 min after G1 release both in the presence and in the absence of replication stress. However, Clb5 levels were stabilized for a longer time in the presence of HU (Clb5 expression decline after 90 min of G1-release without HU versus 150 min in the presence of replication stress) (Figure 3A). Both *MAD2* deletion and *rad53* mutations accelerated Clb5 decline. Indeed, a 60% reduction in Clb5 levels was observed 30 min before in *mad2Δ* and in *rad53-K227A* cells compared to WT. Clb5 reduction was even more pronounced in *rad53-K227A mad2Δ* cells in which Clb5 became hardly detectable. We conclude that both Mad2 and Rad53 contribute to maintain Clb5 levels in the presence of replication stress. Furthermore, their additive effect on Clb5 suggests that Rad53 and Mad2 maintain Clb5 levels through different mechanisms. Similar results were obtained for the other S-phase cyclin, Clb6 (Figure S3A). We note that Mad2 did not affect the general

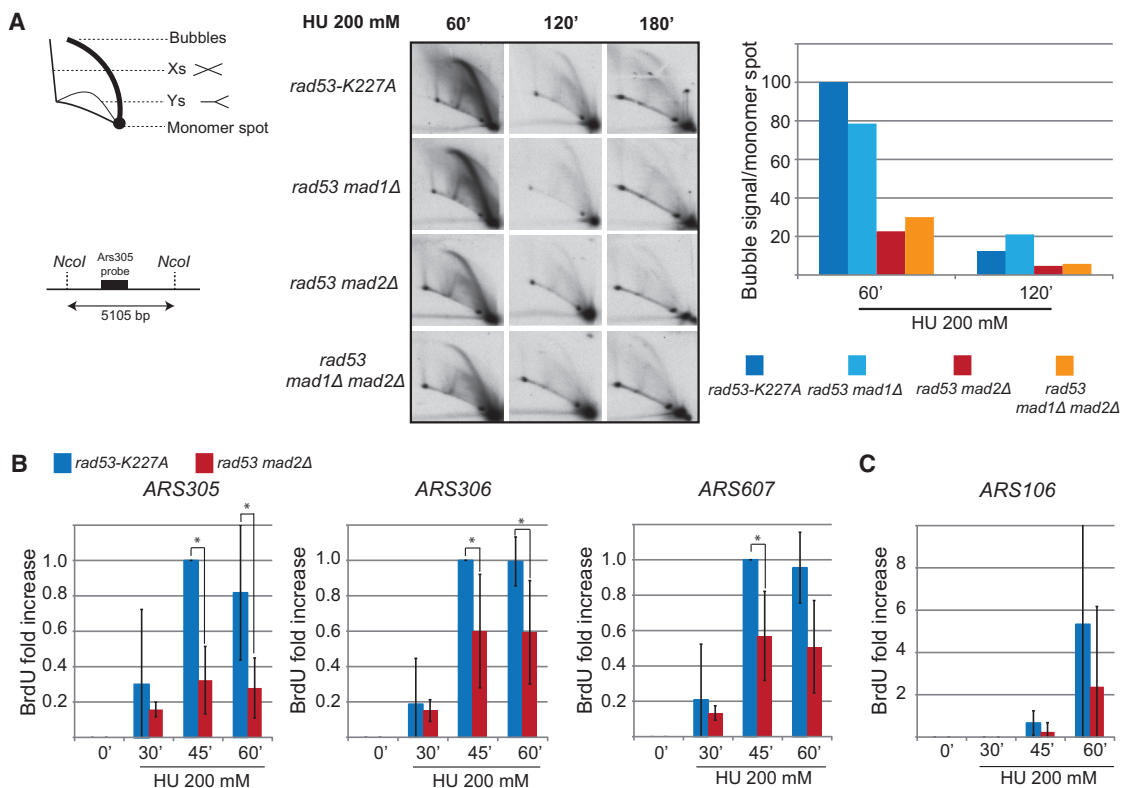


**Figure 2. Mad2 Stimulates Origin Firing in *rad53-K227A* Cells**

(A) 2D gel analysis of replication intermediates in *rad53-K227A*, *rad53-K227A mad1Δ*, *rad53-K227A mad2Δ*, *rad53-K227A mad1Δ mad2Δ* cells at the early origin ARS305. Cells were released from G1 into S-phase at 25°C in 200 mM HU. Quantification of replication intermediates was plotted on the histogram. Intensity of the bubble arc was divided by the intensity of the relative monomer spot, normalized against *rad53-K227A* cells.

(B and C) BrdU immunoprecipitation and quantitative PCR on early (B) and late (C) origins in *rad53-K227A* and *rad53-K227A mad2Δ* cells. Cells were released from G1 into S-phase at 25°C in the presence of 200mM HU and 200 μg/ml BrdU. BrdU fold increase was calculated as a ratio:IP/input, normalized against BrdU signal of *rad53-K227A* cells after 45 min of release. Scale bars represent the SD of three independent experiments. Asterisks indicate statistically significant differences between cell lines (one-tailed Wilcoxon test with a p value ≤ 0.05).

protein expression, since the abundance of the replication factor Orc2, of the cyclin Clb2, or of the housekeeping gene Pgc1, was not reduced by *MAD2* deletion (Figure S3B).

### Rad53 Inhibits Clb5 Degradation under Replication Stress

The decrease in cyclin expression that we have previously observed can result from a defect in transcription, translation, and/or protein degradation. To test the contribution of Rad53 or Mad2 in transcription, WT, *mad2Δ*, *rad53-K227A*, and *rad53-K227A mad2Δ* cells were synchronized in G1 and released into S-phase in the presence of 200 mM HU. mRNA abundance was measured by reverse transcription (RT) and qPCR. As shown in Figure 3C, Clb5 transcription initiates at the end of the G1 phase, 30 min after  $\alpha$  factor release. The levels of Clb5 transcripts were similar in all strains. We conclude that neither *MAD2* deletion nor *rad53* mutation influences Clb5 transcription. Similar results were observed for the other S-phase cyclin, Clb6 (Figures S3C and S3D).

We then investigated whether Mad2 or Rad53 could have an impact on Clb5 degradation. WT, *rad53-K227A*, and *rad53-*

*K227A mad2Δ* cells were synchronized in G1 and released into S-phase in the presence of 200 mM HU and 100 μM MG132, a proteasome inhibitor, which specifically protects short-lived protein from degradation (Lee and Goldberg, 1996). Under MG132 and HU treatment, Clb5 protein levels remained almost constant in WT cells, even after 3 hr of release (Figure 3D). A similar result was observed in *rad53-K227A* cells. While the levels of Clb5 were reduced by 70% after 150 min of release without MG132, Clb5 levels decreased only by 15% during the same period in the presence of MG132 (Figures 3D and S3E). We ruled out a cell-cycle issue, since FACS profiles were comparable with or without MG132 (data not shown).

The same strategy was used to study the contribution of Mad2 to Clb5 degradation. Contrary to what we observed in *rad53-K227A* cells, the level of Clb5 gradually decreased under HU treatment in *rad53-K227A mad2Δ* cells, even in the presence of MG132 (Figure 3D). We conclude that Rad53 protects Clb5 from degradation during HU treatment, while Mad2 acts through a mechanism that is not affected by MG132 treatment.

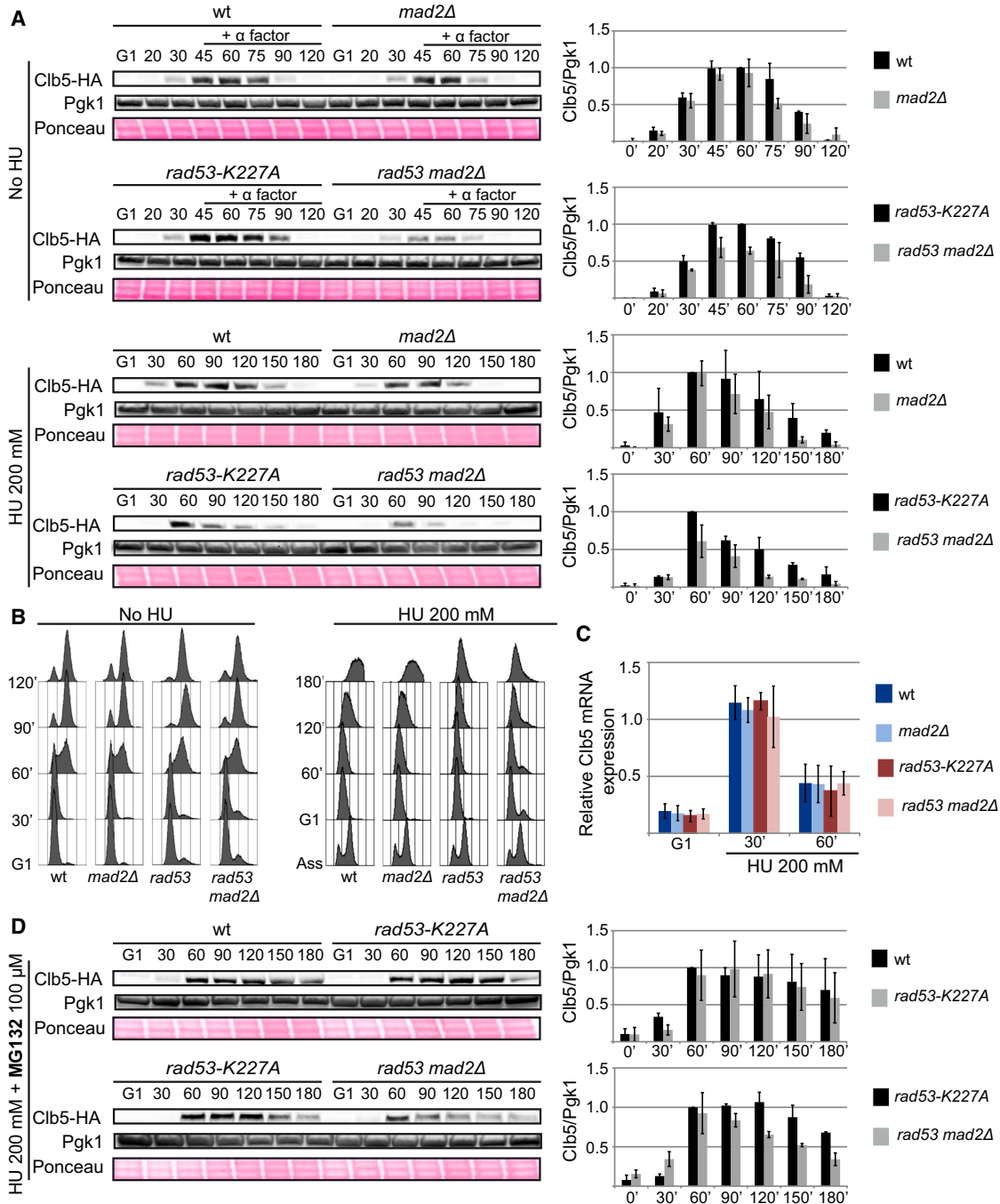


**Figure 3. Rad53 and Mad2 Regulate Clb5 Expression**

(A) Expression of Clb5-HA was followed throughout the cell-cycle progression in WT, *mad2* $\Delta$ , *rad53-K227A*, and *rad53-K227A mad2* $\Delta$  cells by western blot analysis. Pgk1 and Ponceau S were used as loading controls. Cells were released from G1 into S-phase at 25°C in YPD  $\pm$  200 mM HU. In the absence of HU,  $\alpha$  factor was re-added in the medium after 40 min of release in order to avoid cell re-entry into a new cell cycle. Clb5/Pgk1 signal ratio was plotted for each condition, using WT/*rad53-K227A* cells at 60 min as a reference. The error bars represent the SD of two independent experiments.

(B) WT, *mad2* $\Delta$ , *rad53-K227A*, and *rad53-K227A mad2* $\Delta$  cells were released from G1 into S-phase at 25°C in YPD  $\pm$  200 mM HU. The cellular DNA content was determined by FACS analysis at the indicated time points.

(C) Total RNAs were extracted from cells synchronized in G1 or released from G1 into S-phase at 25°C in YPD + 200 mM HU. After reverse transcription, the levels of Clb5 mRNA were determined by quantitative PCR. The ratio between the transcription level of *CLB5* and the average expression of two reporter genes (TAF10 and ALG9) was plotted on a histogram. The error bars represent the SD of two independent experiments.

(legend continued on next page)

### Mad2 Stimulates Clb5 Synthesis through 4E-BP Inhibition

High-throughput screenings performed in yeast, human, and plants have previously uncovered some intriguing physical interactions between Mad2 and translation factors (Table S1). These observations, added to our results, suggest that Mad2 could be implicated in Clb5 mRNA translation. To test this possibility, we quantified the translation rate of Clb5 mRNA in *rad53-K227A* and *rad53-K227A mad2Δ* cells (Figures 4A and S4). Cells were synchronized in G1 and released into S-phase for 45 min in the presence of HU. Cycloheximide was added to freeze the ribosomes onto the translating mRNAs. Cytoplasmic, monosome, and polysome fractions were separated on a sucrose gradient, and mRNA levels in polysomes (high translation) and monosomes (low translation) were measured by RT-qPCR. We observed that the deletion of *MAD2* shifted Clb5 mRNA from heavy polysomes to smaller polysomes and monosomes, confirming that Mad2 may impact the translation process of Clb5 mRNA (Figures 4A and S4). We then investigated whether Mad2 co-sediments with polysomes by performing a western blot analysis on sucrose gradient fractions (Figure 4B). We observed that Mad2 co-fractionated with heavy polysomes in an EDTA- and RNase I-dependent manner (addition of EDTA leads to the separation of the 40S and 60S ribosomal subunits while RNase I is an endoribonuclease that preferentially degrades single strand RNA). This result supports the hypothesis that Mad2 interacts with the translational machinery. Interestingly, in *S. cerevisiae*, two independent screenings identified the translation factor Caf20 as a physical partner of Mad2 (Castelli et al., 2015; Graumann et al., 2004). Caf20 has been identified as a repressor of the cap-dependent translation and as a homolog of the eIF4E binding proteins (4E-BP). Consequently, we investigated whether Mad2 could control Clb5 expression through a Caf20-dependent mechanism. *rad53-K227A*, *rad53-K227A caf20Δ*, *rad53-K227A mad2Δ*, and *rad53-K227A mad2Δ caf20Δ* cells were released from G1 into 200 mM HU. Clb5 expression was analyzed by western blot analysis (Figure 4C). The level of Clb5 protein remained similar in *rad53-K227A* and *rad53-K227A caf20Δ* cells, whereas Clb5 level increased in *rad53-K227A mad2Δ caf20Δ* in comparison of *rad53-K227A mad2Δ* cells. In addition, we found that the deletion of *CAF20* suppressed the effect of *MAD2* deletion on Clb5 mRNA translation (Figure 4A). Altogether, these results show that Mad2 impacts Clb5 mRNA translation in a Caf20-dependent manner.

Since *CAF20* deletion restores the Clb5 expression in *rad53-K227A mad2Δ* cells, we investigated the effect of *CAF20* deletion on replication origin firing and HU resistance. As expected, we observed a global increase in origin firing in *rad53-K227A mad2Δ caf20Δ* cells compared to *rad53-K227A mad2Δ* cells (Figure 4D). In agreement with this result, *CAF20* deletion suppressed the HU sensitivity observed in *rad53-K227A mad2Δ* cells (Figure 4E). Hence, Mad2 inhibits the 4E-BP Caf20, which in turn counteracts Clb5 synthesis and efficient origin firing.

### Mad2 Modifies the Interaction of Caf20 with the Translational Machinery

Mad2 could inhibit Caf20 by at least two different mechanisms: preventing its loading onto mRNA or counteracting its activity. To test the first possibility, *rad53-K227A* and *rad53-K227A mad2Δ* cells were released from G1 into S-phase for 45 min in the presence of HU. Protein complexes were fixed onto mRNA with formaldehyde. mRNAs bound to Caf20-HA were co-immunoprecipitated with an anti-HA antibody, reverse transcribed, and quantified using quantitative PCR. As it was previously described (Castelli et al., 2015; Costello et al., 2015), we found that Caf20 was strongly bound to its own mRNA (Figure S5). In addition, we observed that Clb5 mRNA was also bound by Caf20. We confirmed that this association was specific, since the attachment of Caf20 onto Clb5 mRNA was higher compared to the binding of Caf20 onto a negative control (Alg9 mRNA). However, we found that the deletion of *MAD2* did not significantly modify the recruitment of Caf20 onto Clb5 mRNA. This result implies that Mad2 inhibits Caf20 by a mechanism that is independent of the recruitment of Caf20 onto mRNAs.

We then investigated whether Mad2 could counteract the activity of Caf20 by altering its interaction with the translational machinery. *rad53-K227A* and *rad53-K227A mad2Δ* cells were synchronized in G1 and released into S phase for 45 min in the presence of HU. We did not observe significant differences in Caf20 protein levels by western blotting in the two strains (data not shown). Caf20-HA and its interactors were co-immunoprecipitated. Protein partners were identified and quantified by mass spectrometry. As it was previously described (Costello et al., 2015), we found that Caf20 interacts with a large number of translation factors implicated in both initiation and elongation (Figures 5A and 5B; Table S2). In addition, we observed that, in the absence of Mad2, Caf20 globally increases its association with the whole translational machinery (translational initiation factors and ribosomal proteins). Conversely, only the translational initiation factor eIF4E (Cdc33) reduced its affinity for Caf20 in the absence of Mad2 (Figure 5B). We conclude that Mad2 hinders the stable association between Caf20 and the translation machinery, while it specifically stabilizes the binding of Caf20 with eIF4E.

## DISCUSSION

Many oncogenes and tumor suppressors target cyclins and CDKs. For example, cMyc promotes Cyclin D/E/A transcription (Bretones et al., 2015), while p53 favors the transcription of p21, a CDK inhibitor (Georgakilas et al., 2017). In this study, we uncovered a Mad2-mediated regulatory circuit promoting S-phase cyclin expression. In particular, the levels of Clb5 and Clb6 are compromised when Mad2 is ablated in unperturbed conditions and in response to replication stress. Mad2 is a well-known effector of the spindle checkpoint, but its S-phase function is independent of the other SAC components like

(D) Expression of Clb5-HA upon treatment with a proteasome inhibitor (MG132) was followed throughout the cell-cycle progression in WT, *mad2Δ*, *rad53-K227A*, and *rad53-K227A mad2Δ* cells by western blot analysis. Pgk1 and Ponceau S were used as loading controls. Cells were released from G1 into S-phase at 25°C in YPD + 200 mM HU + 100 μM MG132. Clb5/Pgk1 signal ratio was plotted for each condition, using WT cells at 60 min as a reference. The error bars represent the SD of two independent experiments.

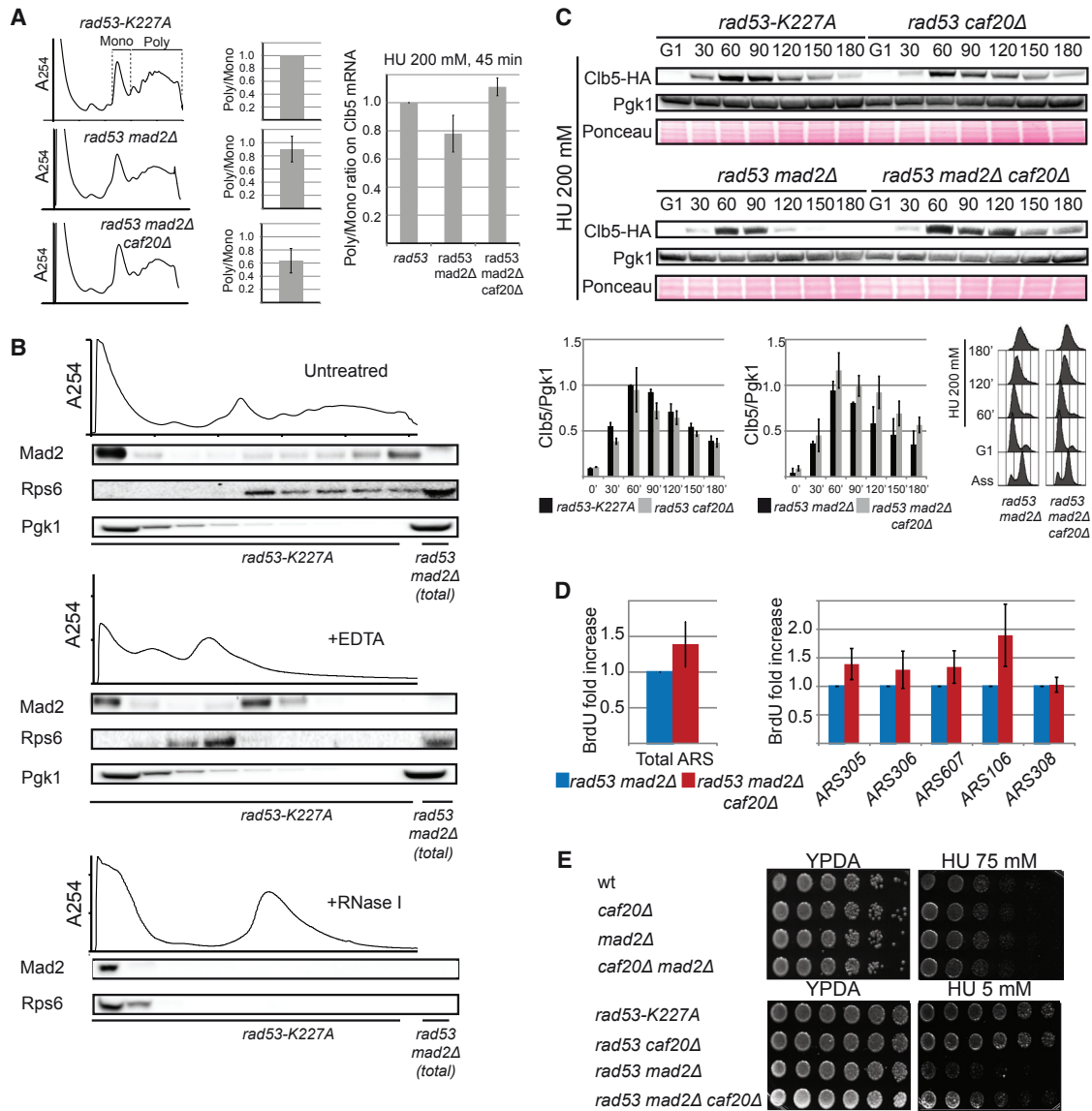


**Figure 4. Mad2 Controls Cib5 mRNA Translation via a Caf20-Dependent Mechanism**

(A) Translational rate of Cib5 mRNA in *rad53-K227A*, *rad53-K227A mad2Δ*, and *rad53-K227A mad2Δ caf20Δ* cells. Cells were released from G1 into 200 mM HU for 45 min at 25°C. Polysome/monosome ratio (Poly/Mono) at the global level or on Cib5 mRNA was plotted for each strain using *rad53-K227A* as a reference. Error bars represent the SD of two independent experiments.

(B) Mad2, Pgk1, and Rps6 protein distribution across the sucrose gradient was analyzed by western blotting in the absence or in the presence of EDTA/RNase I.

(C) Expression of Cib5-HA was followed throughout the cell-cycle progression in *rad53-K227A*, *rad53-K227A caf20Δ*, *rad53-K227A mad2Δ*, and *rad53-K227A mad2Δ caf20Δ* cells by western blot analysis. Pgk1 and Ponceau S were used as loading controls. Cells were released from G1 into 200 mM HU at 25°C. Cib5/Pgk1 signal ratio was plotted for each condition, using *rad53-K227A* and *rad53-K227A mad2Δ* cells at 60 min as a reference. Error bars represent the SD of two independent experiments for *rad53-K227A* versus *rad53-K227A caf20Δ* cells and of three independent experiments for *rad53-K227A mad2Δ* versus *rad53-K227A mad2Δ caf20Δ* cells. Cell-cycle progression of *rad53-K227A mad2Δ* and *rad53-K227A mad2Δ caf20Δ* cells was determined by FACS analysis.

(D) BrdU Immunoprecipitation and quantitative PCR on four early (*ARS305*, *ARS306*, *ARS607*, and *ARS308*) and one late (*ARS106*) origins in *rad53-K227A mad2Δ* and *rad53-K227A mad2Δ caf20Δ* cells. Cells were released from G1 into S-phase for 45 min at 25°C in the presence of 200 mM HU and 200 μg/ml BrdU. BrdU fold increase was calculated as a ratio: IP/input, normalized against BrdU signal of *rad53-K227A mad2Δ*. Error bars represent the SD of two independent experiments.

(E) Cells were spotted in 2-fold serial dilutions on YPDA/HU plates. Relative growth was assayed after 2 days of culture at 28°C. The *rad53-K227A* allele is marked as *rad53*.

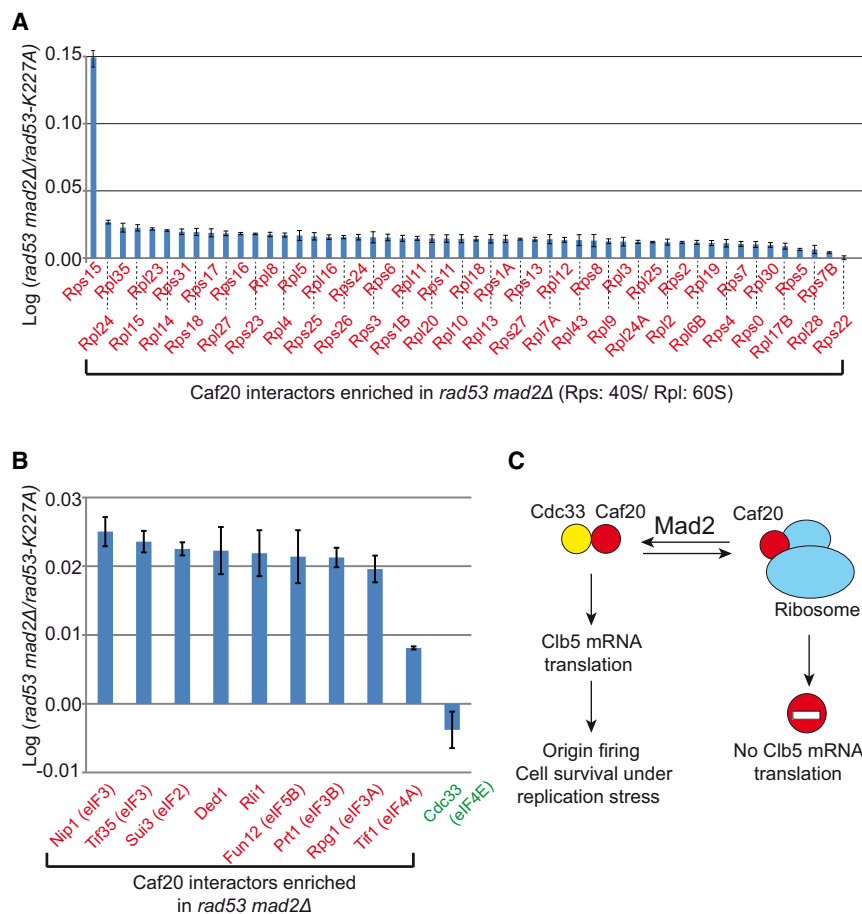


**Figure 5. Mad2 Affects the Recruitment of the Translational Machinery**

(A and B) *rad53-K227A* CAF20-HA, *rad53-K227A mad2Δ* CAF20-HA cells were released from G1 into S-phase at 25°C in 200 mM HU for 45 min. Proteins interacting with Caf20 (A, ribosomal proteins; B, initiator factors) were co-immunoprecipitated using an anti HA antibody and identified by mass spectrometry. Statistically significant differences between *rad53-K227A* and *rad53-K227A mad2Δ* cells were plotted on a logarithmic scale so that higher interaction in *rad53-K227A mad2Δ* cells is shown as a positive number. (Red) Interactors enriched in *rad53-K227A mad2Δ* cells; (green) interactor enriched in *rad53-K227A* cells. (C) Model for the translational regulation of the S-phase cyclin mRNAs by Mad2. Mad2 regulates the affinity of Caf20 for the translational machinery. Mad2 decreases the association Caf20/ribosomes while it stabilizes the association Caf20/Cdc33.

in Clb5 mRNA). We found that Mad2 changes the affinity of Caf20 for its protein partners (Figures 5A and 5B). In the absence of Mad2, the association of Caf20 with the translational machinery increases, probably negatively regulating the translation rate. In parallel, in the absence of Mad2, Caf20 has less affinity for eIF4E (Figure 5C). We have no direct evidence to argue for a competition between eIF4E and the translation machinery, but it is interesting

Mad1, Mad3, and Bub3. Moreover, since Mad1 also favors the proper localization of Mad2 at the kinetochore during mitosis and at the nuclear pore during interphase (Campbell et al., 2001; De Souza et al., 2009; Lee et al., 2008; Lussi et al., 2010), our results imply that the S-phase function of Mad2 influencing Clb5 expression does not depend on its localization at the kinetochore or at the nuclear pores. We ruled out a contribution of Mad2 in promoting Clb5 transcription or in regulating its degradation. Our results rather indicate that Mad2 promotes an optimal Clb5 protein synthesis.

Previous high-throughput studies have already identified some interactions between Mad2 and translational factors (Table S1), and to our knowledge, Mad2 is the only component of the spindle checkpoint which presents such interactions. Here we found that Mad2 co-sediments with translating ribosomes (Figure 4B) and that Mad2 directly promotes the translation of Clb5 mRNA via a Caf20-dependent mechanism (Figure 4A). We observed that Caf20 binds Clb5 mRNA, regardless of the presence or the absence of Mad2 (Figure S5). Recent studies demonstrated that Caf20 is recruited onto mRNAs via its interaction with the eIF4E factor, or via its fixation on the 3'UTR motif present on mRNAs. Interestingly, Clb5 and Clb6 mRNA share the properties of the 4E-independent recruitment. Indeed, both of them present a Caf20 consensus sequence in their 3'UTR ("AUUAUAUGUAUAUA" localized 100 nt after the stop codon

to note that the same tendency has already been observed for a Caf20 mutant that has a defective eIF4E binding (Castelli et al., 2015).

We also found that, in response to replication stress, Rad53 controls Clb5 protein degradation (Figure 3). Interestingly, Clb6 protein degradation upon replication stress is also dependent on Rad53 (Palou et al., 2010). Although Clb5 stabilization occurs in response to both replication stress and intra-S DNA damage (MMS, treatment), the mechanisms seem different (Germain et al., 1997). In particular, the proteolysis inhibition observed in the presence of DNA damage is independent of the checkpoint proteins Mec1 and Rad53 (Germain et al., 1997). This observation could explain why *rad53-K227A mad2Δ* cells are specifically sensitive to HU and not to other DNA damaging agents. Contrary to Rnr1, whose transcription level is maintained during the duration of S-phase upon replication stress through a Rad53 dependent mechanism (Figure S3D; Travesa et al., 2012), we note that we did not find evidence for a contribution of Rad53 in prolonging Clb5 or Clb6 transcription upon replication stress (Figures 3 and S3D).

Importantly, the Rad53-Mad2 synergistic and specific effect in response to replication stress seems to be at least partially conserved between different yeast species. Indeed, previous observations in *S. pombe* also underlined that (1) MAD2 and

*CDS1* (*RAD53* homolog) exhibit a negative genetic interaction in the presence of replication stress; (2) this interaction is specific for *MAD2* over the other components of the spindle checkpoint (*MAD1*, *MAD3*, and *BUB1*); and (3) this interaction is specific to the cellular response to replication stress and not to DNA damage (Sugimoto et al., 2004). However, while in *S. pombe* the APC is hyperactivated in the absence of Mad2, we did not find any increase in APC activity in *S. cerevisiae* (no modification of Clb2 degradation). On the contrary, we proposed that Mad2 interferes with the translation process. It is particularly interesting to note that physical interactions between the spindle checkpoint protein Mad2 and the translational machinery have already been identified in different organisms including plants and humans (Table S1).

The Mad2 function described in our paper may have relevant implications for cancer cells. Expression of SAC proteins is often deregulated in tumor cells. However, Mad2 deregulation is particularly prominent over the other spindle checkpoints proteins. Oncomine database analysis revealed that only 2% of cancer cells show an upregulated expression of Mad1, whereas 18% of cancer cells exhibit Mad2 upregulation. This specific increase is particularly relevant in colorectal cancer, in which one-third of the tumor tissue analyzed exhibits an overexpression of Mad2. An additional role of Mad2 out of the spindle checkpoint could explain the particular prominence of Mad2 deregulation. It is also worth noting that many cancer cells exhibit a delocalization of Mad2 protein from the nucleus to the cytoplasm (Fung et al., 2007; Li et al., 2003), a cellular compartment in which Mad2 is not functional as a spindle checkpoint player (Kasai et al., 2002) but could be fully functional as a regulator of the translation process. Given that differences exist between yeast and mammals at the level of 4E-BP regulation, more work will be required to address whether Mad2 affects protein translation also in mammalian cells.

## STAR★METHODS

Detailed methods are provided in the online version of this paper and include the following:

- KEY RESOURCES TABLE
- CONTACT FOR REAGENT AND RESOURCE SHARING
- EXPERIMENTAL MODEL AND SUBJECT DETAILS
- METHODS DETAILS
  - Drug sensitivity assay
  - Protein extraction and Western Blot analysis
  - 2D Gel Electrophoresis of replication intermediates
  - BrdU immuno-precipitation
  - Quantitative PCR
  - RNA extraction and reverse transcription
  - Fluorescence-activated cell sorter (FACS) analysis
  - Non-denaturing protein Co-immunoprecipitation
  - Mass-spectrometry (MS)
  - RNA co-immunoprecipitation
  - Polysome profiling
  - Quantification and statistical analysis
  - Data and software availability

## SUPPLEMENTAL INFORMATION

Supplemental Information includes five figures and four tables and can be found with this article at <https://doi.org/10.1016/j.molcel.2018.04.020>.

## ACKNOWLEDGMENTS

We thank Dana Branzei, Michelle Debatisse, Michele Giannattasio, Fabio Iannelli, Muege Ogrunc, and Federica Zanardi for the critical reading of the manuscript and suggestions, and Vittoria Matafora for suggestions regarding the statistical analysis of proteomics data. S.G. was supported by postdoctoral fellowships from the Fondazione Veronesi and the Associazione Italiana per la Ricerca sul Cancro. The study was supported by grants from Associazione Italiana per la Ricerca sul Cancro (M.F. and S.B.), Association for International Cancer Research (M.F.), Telethon-Italy (M.F.), CEN-Italy (M.F.), Ministero dell'Istruzione Universitaria e della Ricerca (M.F.), and the European Commission (M.F. and S.B.).

## AUTHOR CONTRIBUTIONS

D.P. and S.G. executed the experiments. C.B., S.R., and S.B. executed and analyzed the polysome profiling experiments. P.S. performed the mass spectrometry analysis. S.G. designed the experiments. W.C., D.P., and S.G. analyzed the data. M.F. and S.G. conceived the project and wrote the article. M.F. provided financial support.

## DECLARATION OF INTERESTS

The authors declare no competing interests.

Received: November 6, 2017

Revised: February 26, 2018

Accepted: April 23, 2018

Published: May 17, 2018

## REFERENCES

- Aravind, L., and Koonin, E.V. (1998). The HORMA domain: a common structural denominator in mitotic checkpoints, chromosome synapsis and DNA repair. *Trends Biochem. Sci.* 23, 284–286.
- Batisse, J., Batisse, C., Budd, A., Böttcher, B., and Hurt, E. (2009). Purification of nuclear poly(A)-binding protein Nab2 reveals association with the yeast transcriptome and a messenger ribonucleoprotein core structure. *J. Biol. Chem.* 284, 34911–34917.
- Bell, S.P., and Dutta, A. (2002). DNA replication in eukaryotic cells. *Annu. Rev. Biochem.* 71, 333–374.
- Bermejo, R., Katou, Y.M., Shirahige, K., and Foiani, M. (2009). ChIP-on-chip analysis of DNA topoisomerases. *Methods Mol. Biol.* 582, 103–118.
- Bermejo, R., Lai, M.S., and Foiani, M. (2012). Preventing replication stress to maintain genome stability: resolving conflicts between replication and transcription. *Mol. Cell* 45, 710–718.
- Branzei, D., and Foiani, M. (2009). The checkpoint response to replication stress. *DNA Repair (Amst.)* 8, 1038–1046.
- Bretones, G., Delgado, M.D., and León, J. (2015). Myc and cell cycle control. *Biochim. Biophys. Acta* 1849, 506–516.
- Brewer, B.J., and Fangman, W.L. (1987). The localization of replication origins on ARS plasmids in *S. cerevisiae*. *Cell* 51, 463–471.
- Cairo, L.V., Ptak, C., and Wozniak, R.W. (2013). Mitosis-specific regulation of nuclear transport by the spindle assembly checkpoint protein Mad1p. *Mol. Cell* 49, 109–120.
- Campbell, M.S., Chan, G.K., and Yen, T.J. (2001). Mitotic checkpoint proteins HsMAD1 and HsMAD2 are associated with nuclear pore complexes in interphase. *J. Cell Sci.* 114, 953–963.
- Castelli, L.M., Talavera, D., Kershaw, C.J., Mohammad-Qureshi, S.S., Costello, J.L., Rowe, W., Sims, P.F., Grant, C.M., Hubbard, S.J., Ashe, M.P.,

- and Pavitt, G.D. (2015). The 4E-BP Caf20p mediates both eIF4E-dependent and independent repression of translation. *PLoS Genet.* *11*, e1005233.
- Costello, J., Castelli, L.M., Rowe, W., Kershaw, C.J., Talavera, D., Mohammad-Qureshi, S.S., Sims, P.F., Grant, C.M., Pavitt, G.D., Hubbard, S.J., and Ashe, M.P. (2015). Global mRNA selection mechanisms for translation initiation. *Genome Biol.* *16*, 10.
- De Souza, C.P., Hashmi, S.B., Nayak, T., Oakley, B., and Osmani, S.A. (2009). Mlp1 acts as a mitotic scaffold to spatially regulate spindle assembly checkpoint proteins in *Aspergillus nidulans*. *Mol. Biol. Cell* *20*, 2146–2159.
- Diffley, J.F., and Labib, K. (2002). The chromosome replication cycle. *J. Cell Sci.* *115*, 869–872.
- Donaldson, A.D., Raghuraman, M.K., Friedman, K.L., Cross, F.R., Brewer, B.J., and Fangman, W.L. (1998). CLB5-dependent activation of late replication origins in *S. cerevisiae*. *Mol. Cell* *2*, 173–182.
- Epstein, C.B., and Cross, F.R. (1992). CLB5: a novel B cyclin from budding yeast with a role in S phase. *Genes Dev.* *6*, 1695–1706.
- Fiorani, S., Mimun, G., Caleca, L., Piccini, D., and Pellicoli, A. (2008). Characterization of the activation domain of the Rad53 checkpoint kinase. *Cell Cycle* *7*, 493–499.
- Foley, E.A., and Kapoor, T.M. (2013). Microtubule attachment and spindle assembly checkpoint signalling at the kinetochore. *Nat. Rev. Mol. Cell Biol.* *14*, 25–37.
- Fraschini, R., Beretta, A., Sironi, L., Musacchio, A., Lucchini, G., and Piatti, S. (2001). Bub3 interaction with Mad2, Mad3 and Cdc20 is mediated by WD40 repeats and does not require intact kinetochores. *EMBO J.* *20*, 6648–6659.
- Fung, M.K., Cheung, H.W., Wong, H.L., Yuen, H.F., Ling, M.T., Chan, K.W., Wong, Y.C., Cheung, A.L., and Wang, X. (2007). MAD2 expression and its significance in mitotic checkpoint control in testicular germ cell tumour. *Biochim. Biophys. Acta* *1773*, 821–832.
- Georgakilas, A.G., Martin, O.A., and Bonner, W.M. (2017). p21: a two-faced genome guardian. *Trends Mol. Med.* *23*, 310–319.
- Germain, D., Hendley, J., and Futcher, B. (1997). DNA damage inhibits proteolysis of the B-type cyclin Clb5 in *S. cerevisiae*. *J. Cell Sci.* *110*, 1813–1820.
- Gibson, D.G., Aparicio, J.G., Hu, F., and Aparicio, O.M. (2004). Diminished S-phase cyclin-dependent kinase function elicits vital Rad53-dependent checkpoint responses in *Saccharomyces cerevisiae*. *Mol. Cell. Biol.* *24*, 10208–10222.
- Godek, K.M., Kabeche, L., and Compton, D.A. (2015). Regulation of kinetochore-microtubule attachments through homeostatic control during mitosis. *Nat. Rev. Mol. Cell Biol.* *16*, 57–64.
- Graumann, J., Dunipace, L.A., Seol, J.H., McDonald, W.H., Yates, J.R., 3rd, Wold, B.J., and Deshaies, R.J. (2004). Applicability of tandem affinity purification MudPIT to pathway proteomics in yeast. *Mol. Cell. Proteomics* *3*, 226–237.
- Gunjan, A., and Verreault, A. (2003). A Rad53 kinase-dependent surveillance mechanism that regulates histone protein levels in *S. cerevisiae*. *Cell* *115*, 537–549.
- Hanafusa, T., Habu, T., Tomida, J., Ohashi, E., Murakumo, Y., and Ohmori, H. (2010). Overlapping in short motif sequences for binding to human REV7 and MAD2 proteins. *Genes Cells* *15*, 281–296.
- Hsu, W.S., Erickson, S.L., Tsai, H.J., Andrews, C.A., Vas, A.C., and Clarke, D.J. (2011). S-phase cyclin-dependent kinases promote sister chromatid cohesion in budding yeast. *Mol. Cell. Biol.* *31*, 2470–2483.
- Jackson, L.P., Reed, S.I., and Haase, S.B. (2006). Distinct mechanisms control the stability of the related S-phase cyclins Clb5 and Clb6. *Mol. Cell. Biol.* *26*, 2456–2466.
- Kasai, T., Iwanaga, Y., Iha, H., and Jeang, K.T. (2002). Prevalent loss of mitotic spindle checkpoint in adult T-cell leukemia confers resistance to microtubule inhibitors. *J. Biol. Chem.* *277*, 5187–5193.
- Katou, Y., Kanoh, Y., Bando, M., Noguchi, H., Tanaka, H., Ashikari, T., Sugimoto, K., and Shirahige, K. (2003). S-phase checkpoint proteins Tof1 and Mrc1 form a stable replication-pausing complex. *Nature* *424*, 1078–1083.
- Krakov, I.H., Brown, N.C., and Reichard, P. (1968). Inhibition of ribonucleoside diphosphate reductase by hydroxyurea. *Cancer Res.* *28*, 1559–1565.
- Lee, D.H., and Goldberg, A.L. (1996). Selective inhibitors of the proteasome-dependent and vacuolar pathways of protein degradation in *Saccharomyces cerevisiae*. *J. Biol. Chem.* *271*, 27280–27284.
- Lee, S.H., Sterling, H., Burlingame, A., and McCormick, F. (2008). Tpr directly binds to Mad1 and Mad2 and is important for the Mad1-Mad2-mediated mitotic spindle checkpoint. *Genes Dev.* *22*, 2926–2931.
- Lengronne, A., Pasero, P., Bensimon, A., and Schwob, E. (2001). Monitoring S phase progression globally and locally using BrdU incorporation in TK(+) yeast strains. *Nucleic Acids Res.* *29*, 1433–1442.
- Li, G.Q., Li, H., and Zhang, H.F. (2003). Mad2 and p53 expression profiles in colorectal cancer and its clinical significance. *World J. Gastroenterol.* *9*, 1972–1975.
- Lopes, M., Cotta-Ramusino, C., Pellicoli, A., Liberi, G., Plevani, P., Muzi-Falconi, M., Newlon, C.S., and Foiani, M. (2001). The DNA replication checkpoint response stabilizes stalled replication forks. *Nature* *412*, 557–561.
- Lussi, Y.C., Shumaker, D.K., Shimi, T., and Fahrenkrog, B. (2010). The nucleoporin Nup153 affects spindle checkpoint activity due to an association with Mad1. *Nucleus* *1*, 71–84.
- Manfrini, N., Gobbini, E., Baldo, V., Trovesi, C., Lucchini, G., and Longhese, M.P. (2012). G(1)/S and G(2)/M cyclin-dependent kinase activities commit cells to death in the absence of the S-phase checkpoint. *Mol. Cell. Biol.* *32*, 4971–4985.
- Marheineke, K., and Hyrien, O. (2004). Control of replication origin density and firing time in *Xenopus* egg extracts: role of a caffeine-sensitive, ATR-dependent checkpoint. *J. Biol. Chem.* *279*, 28071–28081.
- Musacchio, A. (2015). The molecular biology of spindle assembly checkpoint signaling dynamics. *Curr. Biol.* *25*, R1002–R1018.
- Palou, G., Palou, R., Guerra-Moreno, A., Duch, A., Travesa, A., and Quintana, D.G. (2010). Cyclin regulation by the s phase checkpoint. *J. Biol. Chem.* *285*, 26431–26440.
- Pellicoli, A., Lucca, C., Liberi, G., Marini, F., Lopes, M., Plevani, P., Romano, A., Di Fiore, P.P., and Foiani, M. (1999). Activation of Rad53 kinase in response to DNA damage and its effect in modulating phosphorylation of the lagging strand DNA polymerase. *EMBO J.* *18*, 6561–6572.
- Santocanele, C., and Diffley, J.F. (1998). A Mec1- and Rad53-dependent checkpoint controls late-firing origins of DNA replication. *Nature* *395*, 615–618.
- Schuyler, S.C., Wu, Y.F., and Kuan, V.J. (2012). The Mad1-Mad2 balancing act—a damaged spindle checkpoint in chromosome instability and cancer. *J. Cell Sci.* *125*, 4197–4206.
- Shirayama, M., Tóth, A., Gálová, M., and Nasmyth, K. (1999). APC(Cdc20) promotes exit from mitosis by destroying the anaphase inhibitor Pds1 and cyclin Clb5. *Nature* *402*, 203–207.
- Soffientini, P., and Bachi, A. (2016). STAGE-digging: A novel in-gel digestion processing for proteomics samples. *J. Proteomics* *140*, 48–54.
- Sogo, J.M., Lopes, M., and Foiani, M. (2002). Fork reversal and ssDNA accumulation at stalled replication forks owing to checkpoint defects. *Science* *297*, 599–602.
- Sudakin, V., Chan, G.K., and Yen, T.J. (2001). Checkpoint inhibition of the APC/C in HeLa cells is mediated by a complex of BUBR1, BUB3, CDC20, and MAD2. *J. Cell Biol.* *154*, 925–936.
- Sugimoto, I., Murakami, H., Tonami, Y., Moriyama, A., and Nakanishi, M. (2004). DNA replication checkpoint control mediated by the spindle checkpoint protein Mad2p in fission yeast. *J. Biol. Chem.* *279*, 47372–47378.
- Suijkerbuijk, S.J., and Kops, G.J. (2008). Preventing aneuploidy: the contribution of mitotic checkpoint proteins. *Biochim. Biophys. Acta* *1786*, 24–31.
- Teste, M.A., Duquenne, M., François, J.M., and Parrou, J.L. (2009). Validation of reference genes for quantitative expression analysis by real-time RT-PCR in *Saccharomyces cerevisiae*. *BMC Mol. Biol.* *10*, 99.
- Travesa, A., Kuo, D., de Bruin, R.A., Kalashnikova, T.I., Guaderrama, M., Thai, K., Aslanian, A., Smolka, M.B., Yates, J.R., 3rd, Ideker, T., and Wittenberg, C.

- (2012). DNA replication stress differentially regulates G1/S genes via Rad53-dependent inactivation of Nrm1. *EMBO J.* *31*, 1811–1822.
- Uetz, P., Giot, L., Cagney, G., Mansfield, T.A., Judson, R.S., Knight, J.R., Lockshon, D., Narayan, V., Srinivasan, M., Pochart, P., et al. (2000). A comprehensive analysis of protein-protein interactions in *Saccharomyces cerevisiae*. *Nature* *403*, 623–627.
- Vernieri, C., Chiroli, E., Francia, V., Gross, F., and Ciliberto, A. (2013). Adaptation to the spindle checkpoint is regulated by the interplay between Cdc28/Clbs and PP2ACdc55. *J. Cell Biol.* *202*, 765–778.
- Wäsch, R., and Cross, F.R. (2002). APC-dependent proteolysis of the mitotic cyclin Clb2 is essential for mitotic exit. *Nature* *418*, 556–562.
- Wong, J., Nakajima, Y., Westermann, S., Shang, C., Kang, J.S., Goodner, C., Houshmand, P., Fields, S., Chan, C.S., Drubin, D., et al. (2007). A protein interaction map of the mitotic spindle. *Mol. Biol. Cell* *18*, 3800–3809.
- Yu, H., Braun, P., Yildirim, M.A., Lemmens, I., Venkatesan, K., Sahalie, J., Hirozane-Kishikawa, T., Gebreab, F., Li, N., Simonis, N., et al. (2008). High-quality binary protein interaction map of the yeast interactome network. *Science* *322*, 104–110.
- Zhao, X., and Rothstein, R. (2002). The Dun1 checkpoint kinase phosphorylates and regulates the ribonucleotide reductase inhibitor Sml1. *Proc. Natl. Acad. Sci. USA* *99*, 3746–3751.
- Zhao, X., Muller, E.G., and Rothstein, R. (1998). A suppressor of two essential checkpoint genes identifies a novel protein that negatively affects dNTP pools. *Mol. Cell* *2*, 329–340.
- Zheng, P., Fay, D.S., Burton, J., Xiao, H., Pinkham, J.L., and Stern, D.F. (1993). SPK1 is an essential S-phase-specific gene of *Saccharomyces cerevisiae* that encodes a nuclear serine/threonine/tyrosine kinase. *Mol. Cell. Biol.* *13*, 5829–5842.

## STAR★METHODS

## KEY RESOURCES TABLE

REAGENT or RESOURCE	SOURCE	IDENTIFIER
<b>Antibodies</b>		
Mouse monoclonal anti-phosphorylated Rad53	In house (Fiorani et al., 2008)	Clone F9
Mouse monoclonal anti-phosphorylated histone H2X (ser139)	Merck	Clone JBW301 Cat #05-636
Mouse monoclonal anti-Pgk1	ThermoFisher Scientific	Clone 22C5D8 Cat #459250
Rabbit polyclonal anti-Clb2	Santa-Cruz Biotechnology	Cat #sc9071
Mouse monoclonal anti c-MYC (clone 9E10)	Santa Cruz Biotechnology	Cat #sc-40
Mouse monoclonal anti HA	Biologend	Clone 16B12 Cat #901503
Mouse monoclonal anti BrdU	MBL	Clone 2B1 Cat #MI-11-3
Rabbit polyclonal anti Mad2	In house (Vernieri et al., 2013)	Clone IEO447SI353F
Rabbit polyclonal anti Rps6	ABCam	Cat #ab40820
Goat anti-Mouse IgG (H + L)-HRP Conjugate	Bio-Rad	Cat #1706516
Goat anti-Rabbit IgG (H + L)-HRP Conjugate	Bio-Rad	Cat #1706515
<b>Chemicals, Peptides, and Recombinant Proteins</b>		
Hydroxyurea	Sigma-Aldrich	Cat #H8627
Methyl methanesulfonate (MMS)	Sigma-Aldrich	Cat #129925
MG132	Sigma-Aldrich	Cat #M8699
Cicloheximide	Sigma-Aldrich	Cat #C7698
Camptothecin	Sigma-Aldrich	Cat #208925
Anti-HA.11 Epitope Tag Affinity Matrix	Biologend	Cat #900801
Dynabeads Protein A	ThermoFisher Scientific	Cat #10001D
<b>Critical Commercial Assays</b>		
Genomic DNA buffer genomic set	QIAGEN	Cat #19060
Genomic tip 100/G	QIAGEN	Cat #10243
Rneasy Mini Kit	QIAGEN	Cat #74104
PCR purification kit	QIAGEN	Cat #28106
QuantiFast SYBR green PCR kit	QIAGEN	Cat #204054
<b>Deposited Data</b>		
Proteomic raw data	Peptide Atlas repository	<a href="http://www.peptideatlas.org/PASS/PASS01156">http://www.peptideatlas.org/PASS/PASS01156</a>
Raw Data	Mendeley Data	<a href="http://dx.doi.org/10.17632/wwcrg942cf.1">http://dx.doi.org/10.17632/wwcrg942cf.1</a>
<b>Experimental Models: Organisms/Strains</b>		
All <i>Saccharomyces cerevisiae</i> yeast strains used in this study were W303 derivatives; they are listed in Table S3	This study	N/A
<b>Oligonucleotides</b>		
See Table S4 for a list of oligonucleotides used in this study	Sigma-Aldrich	N/A
<b>Recombinant DNA</b>		
pCH12 ( <i>GAL1- rad53-D339A</i> )	Pelliccioli et al., 1999	N/A

(Continued on next page)

**Continued**

REAGENT or RESOURCE	SOURCE	IDENTIFIER
Software and Algorithms		
Image Quant software	GE Healthcare	<a href="https://www.gelifesciences.com/shop/protein-analysis/molecular-imaging-for-proteins/imaging-software/imagequant-tl-8-1-p-00110?current=29000737">https://www.gelifesciences.com/shop/protein-analysis/molecular-imaging-for-proteins/imaging-software/imagequant-tl-8-1-p-00110?current=29000737</a>
Image Lab software	Bio-Rad	<a href="http://www.bio-rad.com/en-ch/product/image-lab-software">http://www.bio-rad.com/en-ch/product/image-lab-software</a>
Perseus	Max Planck Institute	<a href="http://www.perseus-framework.org">http://www.perseus-framework.org</a>
CellQuest	BD Biosciences	<a href="http://www.bd.com/en-uk/products/molecular-diagnostics/cytometric-analysis-products">http://www.bd.com/en-uk/products/molecular-diagnostics/cytometric-analysis-products</a>

**CONTACT FOR REAGENT AND RESOURCE SHARING**

Further information and requests for resources and reagents should be directed to and will be fulfilled by the Lead Contact, Marco Foiani ([marco.foiani@ifom.eu](mailto:marco.foiani@ifom.eu)).

**EXPERIMENTAL MODEL AND SUBJECT DETAILS**

The list of yeast strains used in this study is available in the [Key Resources Table \(Table S3\)](#). Yeast strains are derived from W303 background (*S. cerevisiae*). All strains, except *cdc33* mutants, are corrected with the wild-type RAD5 locus. Gene deletions and carboxy-terminal tags were carried out using a standard PCR-based strategy to amplify resistance cassettes with appropriate flanking sequences, and replacing the target gene by homologous recombination. All strains, except *rad53-D339A* mutants, carry a repetition of the thymidine kinase (TK) at the URA3 locus in order to allow BrdU incorporation ([Lengronne et al., 2001](#)). *GAL1-rad53-D339A* plasmid was previously described in ([Pelliccioli et al., 1999](#)). Strains were grown at 25°C in yeast extract/peptone with 2% glucose (YPD) or in synthetic complete medium lacking uracil. Exponentially growing cells ( $10^7$  cells/ml) were arrested in G1 using  $\alpha$  factor (5  $\mu$ g/ml). Before release, cells were washed in YP. HU was added at 0.2M, BrdU at 0.2mg/ml and MG132 at 100  $\mu$ M.

**METHODS DETAILS****Drug sensitivity assay**

Cells were grown in liquid culture overnight, counted, adjusted to  $8 \times 10^7$  cells/ml and diluted before being spotted on YPD plates supplemented with adenine (YPDA) containing indicated concentrations of HU, MMS or Camptothecin. Plates were incubated for 2 days at 28°C. Note that serial dilutions of 1:2 were made for *rad53* mutant cells plated on HU while serial dilutions of 1:5 were made in all other cases. *rad53-D339A* mutants were spotted on synthetic growth medium plates deprived of uracil to maintain the plasmid selection.

**Protein extraction and Western Blot analysis**

Protein extracts for western blotting were prepared following cell fixation using trichloroacetic acid and analyzed by SDS-polyacrylamide gel electrophoresis (gel 4/15% Criterion TGX, Biorad). Briefly, cells were quickly spun down and the pellet was resuspended in 20% TCA and lysed by bead beating. Lysate and precipitate/debris was mixed with 200  $\mu$ L 5% TCA and pelleted. The pellet was resuspended in 100  $\mu$ L Laemmli buffer 1X ( $\beta$ -mercaptoethanol as reducing agent) and 50  $\mu$ L Tris base 1M, boiled for 5 min. After centrifugation, the supernatant was transferred in new tubes.

Antibodies used for detection are listed in the [Key Resources Table](#). Detection was done through electrogenerated chemiluminescence (ECL, GE- Healthcare). Quantification was done using Image Lab software (Bio-Rad).

**2D Gel Electrophoresis of replication intermediates**

200ml of exponentially growing cell culture was harvested in the presence of 1% sodium azide and cooled on ice for 15 minutes. Cells were then subjected to *in vivo* psoralen cross-linking. Briefly, cells were washed, resuspended in 5ml of cold water in small Petri dishes and kept on ice. 300  $\mu$ L of 4,5',8-tri-methyl-psoralen solution (0.2 mg/ml in EtOH 100%) was added prior to extensive resuspension by pipetting, followed by 5 min of incubation in the dark and then 10 min of UV irradiation at 365 nm (Stratagene UV Stratalinker). The procedure was repeated 3 times. Cells were centrifuged and resuspended in 5ml of nuclear isolation buffer (17% glycerol, 50mM MOPS, 2mM MgCl<sub>2</sub>, 150mM Kacetate, 0.5mM spermidine, 0.15mM spermine, pH 7.2) and mechanically lysed using an equal volume of glass beads (Sigma, G8772). After centrifugation (8000 rpm, 10 min, 4°C), the pellet was resuspended in 5ml

of G2 buffer (Genomic extraction kit, QIAGEN). Genomic DNA extraction was performed according to manufacturer recommendations. 4  $\mu\text{g}$  of genomic DNA was digested overnight with 200 units of *NcoI* enzyme and then precipitated with 1/8 volume of Kacetate and one volume of isopropanol. Signals were detected following 2D gel electrophoresis (Brewer and Fangman, 1987) and standard Southern blot procedures using a probe against *ARS305* (Chr III 39002-40063). Quantification of bubble arc signal was performed using the Image Quant software (GE Healthcare).

### BrdU immuno-precipitation

150 mL of exponentially cell culture was synchronized in G1, released into S-phase in the presence of 200mM HU and 200  $\mu\text{g}/\text{ml}$  BrdU. At different time points, cells were harvested in the presence of 1% sodium azide and cooled on ice for 15 minutes. Cells were then washed in 20ml of TE and the genomic DNA was extracted using the Genomic extraction kit (QIAGEN) according to manufacturer recommendations. BrdU immuno-precipitations were performed as previously described (Bermejo et al., 2009; Katou et al., 2003). DNA was then resuspended overnight in 250  $\mu\text{L}$  of TE and then sheared using the Bandelin UW2070 sonicator (6 pulses, 20% power, 20 s/pulse). Immediately before immunoprecipitation, the genomic DNA was denatured at 100°C for 10 minutes, cooled immediately on ice and supplemented with 100  $\mu\text{L}$  of ice cold PBS 2x and 200  $\mu\text{L}$  of ice cold-PBS 1X-2% BSA-0,2% Tween20. BrdU immunoprecipitation was carried out overnight using 14  $\mu\text{g}$  of genomic DNA, 20  $\mu\text{L}$  of Protein A-magnetic Dynabeads (Thermo-fisher) and 4  $\mu\text{g}$  of anti-BrdU antibody (clone 2B1, MBL, MI-11-3). 700ng of DNA was kept as an input. After immuno-precipitation, beads were washed 2 times with ice cold lysis buffer (50mM HEPES-KOH pH7.5, 140mM NaCl, 1mM EDTA, 1% Triton x100, 0.1% Na-deoxycholate), 2 times with ice-cold lysis buffer + 500mM NaCl, 2 times with ice-cold washing buffer (10mM Tris-HCl pH8.0, 250mM LiCl, 0.5% NP40, 0.5% Na-deoxycholate, 1mM EDTA) and once with TE. Beads were then resuspended in 50  $\mu\text{L}$  of elution buffer (50 mM Tris-HCl pH8, 10 mM EDTA, 1% SDS), incubated at 65°C for 10 minutes with shaking. After centrifugation and magnetic attachment, the supernatant was transferred into a new tube. 49  $\mu\text{L}$  of TE and 1  $\mu\text{L}$  of proteinase K 50 mg/ml was added to both IP and input tubes. Tubes were incubated at least 2 hours at 37°C. DNA was then purified using the PCR purification Kit (QIAGEN), eluted in 50  $\mu\text{L}$  of the elution buffer of the kit and precipitated at  $-20^\circ\text{C}$  overnight in the presence of 40mM Na- acetate, 1  $\mu\text{L}$  of glycogen and 132.5  $\mu\text{L}$  of 100% ethanol. After centrifugation, the pellet was washed in 70% ethanol, dried and resuspended in 50  $\mu\text{L}$  of bi-distilled water. Input DNA was diluted 50 times and IP DNA 10 times before quantitative PCR.

### Quantitative PCR

Primers used for quantitative PCR are listed in Table S4. Quantitative PCR was prepared using QuantiFast SYBR green PCR kit (QIAGEN) and run on the Lightcycler 480II (Roche) according to the manufacturer's recommendations. Absolute DNA quantification was deduced from standard curve (100; 10; 1 and 0.1ng of input DNA).

### RNA extraction and reverse transcription

Total mRNAs were extracted from  $2.5 \times 10^7$  cells using the RNeasy mini kit (QIAGEN). Reverse transcription was performed using the SuperScript VIL0 cDNA synthesis kit (Invitrogen) with 2  $\mu\text{g}$  of total RNA as starting material. 1/160 of the cDNA reaction was used for quantitative PCR. Two reporter genes (TAF10, ALG9) were chosen for their robustness (Teste et al., 2009) and their distance from replication origins (minimum 12 kb). Normalization was done by dividing the expression of the gene of interest by the average of the two reporter genes.

### Fluorescence-activated cell sorter (FACS) analysis

$1 \times 10^7$  cells were collected by centrifugation, and resuspended overnight in 70% ethanol/ 250mM Tris-HCl (pH 7.5) solution. Cells were then centrifuged and resuspended in 0.5M Tris-HCl (pH 7.5), resuspended in the same buffer containing 2 mg/ml of RNaseA and incubated at 37°C for at least 2h. Cells were then resuspended in 500  $\mu\text{L}$  of 200mM Tris-HCl (pH 7.5), 200mM NaCl, 80mM  $\text{MgCl}_2$  supplemented by 50  $\mu\text{g}/\text{ml}$  of propidium-iodide (Sigma). Samples were then diluted 10-fold in 50mM Tris-HCl (pH 7.5) and analyzed using a Becton Dickinson FACScan and the Cellquest software.

### Non-denaturing protein Co-immunoprecipitation

$2 \times 10^9$  cells were used for each immunoprecipitation. Cell pellet was washed two times in 50ml of TE, and resuspended in 1.6ml of JS buffer (35mM HEPES pH7.5, 105mM NaCl, 0.7% glycerol; 0.7% Triton, 1 mM  $\text{MgCl}_2$ , 3.5mM EDTA, 1 tablet of Phostop-phosphatase inhibitor Roche, 1 tablet of Ultra-protease inhibitor-Roche). The same quantity of zirconium beads was added to the cell suspension and cells were mechanically disrupted at 4°C thanks to the use of a bead-beater. Cell lysate was collected using a gel tip (thin diameter to avoid beads) and proteins were quantified using the Bradford Protein Assay (Biorad). Proteins associated to Caf20-HA were immunoprecipitated overnight using 80  $\mu\text{L}$  of Sepharose beads covalently coupled to an anti-HA antibody (Biolegend). After immunoprecipitation, beads were washed once with JS buffer, two times with JS buffer supplemented with 350 mM NaCl, and two times with JS buffer. At the last step, beads were resuspended in 40  $\mu\text{L}$  of Laemmli buffer, boiled during 6 minutes at 98°C, and centrifuged. The supernatant was analyzed by SDS-polyacrylamide gel electrophoresis. Note that pre-lubricated tubes were used at all stages to avoid protein adherence.

## Mass-spectrometry (MS)

### Protein digestion and peptide preparation

Gel lanes were processed according to STAGE-digging protocol (Soffientini and Bachi, 2016). The entire protocol occurs in a p1000 tip (Sarstedt 70.762.100) filled at the orifice with a double C18 Empore Disk (3M, Minneapolis, MN) plug, named STAGE-digging tip. Briefly, after Coomassie staining, the entire lane was carefully cut into  $\sim 1 \text{ mm}^3$  cubes and transferred into the STAGE-digging tip. These gel cubes were dehydrated with 100% acetonitrile (CAN, Carlo Erba) and rehydrated in 100 mM  $\text{NH}_4\text{HCO}_3$  (Sigma) twice before being dehydrated by the addition of ACN. To ensure that the gel pieces do not create a sticky surface on the C18, all the solutions were added with a gel-loader tip. The removal of solutions was accomplished by centrifugation at 1800 rpm using the commercial tip box as holder. Reduction of protein disulfide bonds was carried out with 10 mM dithiothreitol (DTT) in 100 mM  $\text{NH}_4\text{HCO}_3$  and subsequent alkylation was performed with 55 mM iodoacetamide (IAA) (Sigma), in complete darkness, in 100 mM  $\text{NH}_4\text{HCO}_3$  at room temperature for 30 min. Both DTT and IAA were removed by centrifugation or by syringe as previously described. The gel pieces were rehydrated and dehydrated with 100 mM  $\text{NH}_4\text{HCO}_3$  and ACN respectively prior to digestion. Gel pieces were rehydrated with 40  $\mu\text{L}$  of Trypsin (12.5 ng/ $\mu\text{L}$  in 100 mM  $\text{NH}_4\text{HCO}_3$ ), after few minutes 60  $\mu\text{L}$  of  $\text{NH}_4\text{HCO}_3$  were added and samples were incubated at 37°C o/n in a commercial tip box filled with water on the bottom to ensure that buffer will not evaporate. The digestion solution was then forced through the double plug with a syringe and the flow through was collected. Samples were acidified with 100  $\mu\text{L}$  of 0.1% formic acid (FA, Fluka), forced with the syringe and collected as flow-through. In this way the desalting of peptides occurs. Peptides were eluted twice by adding 100  $\mu\text{L}$  of a solution composed of 80% ACN, 0.1% FA, an extra step of extraction with 100% ACN was performed and then all the eluates were dried in a Speed-Vac and resuspended in 15  $\mu\text{L}$  of solvent A (2% ACN, 0.1% formic acid). 3  $\mu\text{L}$  were injected for each technical replicate on the Q-Exactive –HF mass spectrometer.

### MS analysis and proteins quantification

Mass spectrometry analysis was carried out by LC–MS–MS on a quadrupole Orbitrap Q Exactive HF mass spectrometer (Thermo Scientific). Peptide separation was achieved on a linear gradient from 95% Solvent A to 50% Solvent B (80% acetonitrile, 0.1% formic acid) over 20 min and from 50% to 100% Solvent B in 2 min at a constant flow rate of 0.25  $\mu\text{L min}^{-1}$  on a UHPLC Easy-nLC 1000 (Thermo Scientific), where the LC system was connected to a 25 cm fused-silica emitter of 75  $\mu\text{m}$  inner diameter (New Objective), packed in house with ReproSil-Pur C18-AQ 1.9  $\mu\text{m}$  beads (Maisch) using a high-pressure bomb loader (Proxeon). MS data were acquired using a data-dependent top15 method for HCD fragmentation.

Survey full scan MS spectra (300–1750 Th) were acquired in the Orbitrap with 60,000 resolution, AGC target 1e6, IT 120 ms. For HCD spectra the resolution was set to 15,000, AGC target 1e5, IT 120 ms; normalized collision energy 28 and isolation width 3.0  $m/z$ .

2 technical replicas of each sample were carried out. Raw data were processed with MaxQuant version 1.5.2.8. Peptides were identified from the MS–MS spectra searched against the uniprotKB\_S. *Cerevisiae* database (3845 entries canonical + isoforms) using the Andromeda search engine, in which trypsin specificity was used with up to two missed cleavages allowed.

Cysteine carbamidomethylation was used as a fixed modification, methionine oxidation and protein amino-terminal acetylation as variable modifications. The mass deviation for MS and MS–MS peaks was set at 4.5 and 20 ppm respectively. The peptide and protein false discovery rates (FDRs) were set to 0.01; the minimal length required for a peptide was six amino acids; a minimum of two peptides and at least one unique peptide were required for high-confidence protein identification. The lists of identified proteins were filtered to eliminate reverse hits and known contaminants.

Label-free analysis was carried out, including a ‘match between runs’ option (time window of 5 min). A minimum ratio count of 2 was considered and the ‘LFQ intensities’, which are the intensity values normalized across the entire dataset, were used. 2 Biological and 2 technical replicates for every condition were submitted in a single MaxQuant run.

Statistical t test analyses were done using the Perseus program (Version 1.5.1.6) in the MaxQuant environment. For all the statistical analysis an FDR 0.05 was applied using a permutation test (500 randomizations) and  $S_0 = 1$ .

Gene ontology annotation for biological process and molecular function was manually added by [uniprot.org](http://uniprot.org). Proteins belonging to translational process and ribosomal assembly (list of GO selected is reported in the [Table S2](#), sheet Go\_table) were filtered and only proteins with a valid ratio in both biological replicates were selected.

Ratios of the 2 biological replicates were averaged and plotted in logarithmic scale. Standard deviations were calculated and represented on the plot.

### RNA co-immunoprecipitation

$2 \times 10^9$  cells were used for each immunoprecipitation. Proteins were fixed onto RNA with 1% formaldehyde at 4°C. *In vivo* crosslinking was stopped by addition of 0.1M glycine. Cells were washed four times with 20mL of water. After centrifugation, the cell pellet was resuspended in 0.8ml of Buffer A (20mM Tris-HCl pH8, 140mM NaCl, 1 mM  $\text{MgCl}_2$ , 0.5 mM DTT, 1 tablet of Phostop-phosphatase inhibitor Roche, 1 tablet of Ultra-protease inhibitor-Roche, and 80U/ml RNasin-Promega). The same quantity of zirconium oxide beads was added to the cell suspension and cells were mechanically lysed thanks to the use of a bead-beater. The lysate was recovered with a gel tip (to avoid beads) and centrifuged. Proteins of the supernatant were quantified using the Bradford Protein Assay (Biorad). 20mg of protein extract and 120  $\mu\text{L}$  of Sepharose beads coupled with anti-HA antibody were used for overnight immunoprecipitation. 1mg of protein extract was kept as an input. After immunoprecipitation, beads were washed 3 times shortly with Buffer A, two times 15 minutes with Buffer A, and three times with the Rnase III buffer (10mM Tris-HCl pH8, 10mM  $\text{MgCl}_2$ , 60mM NaCl, 1mM DTT, 10U/ml RNasin-Promega). At the final wash, beads were resuspended in 100  $\mu\text{L}$  of Rnase III buffer supplemented

by 40U RNasin, 1U DNase I, 2U RNase III, and incubate 10 minutes at 37°C. RNase III was deactivated by addition of 900  $\mu$ L of Buffer E (20mM Tris-HCl pH8, 140mM NaCl, 0.5% NP40, 1mM EDTA, 0.5 mM DTT, 40U/ml RNasin-Promega). Beads were further washed three more times with buffer E. At the last wash, beads were resuspended in 270  $\mu$ L of proteinase K buffer (10mM Tris-HCl pH8, 200mM NaCl, 1mM EDTA, 0.1% SDS, 10U/ml RNasin-Promega). Proteinase K buffer up to 270  $\mu$ L was also added to the input samples. 50  $\mu$ g of proteinase was added to IP and input and the samples were incubated for two hours at 40°C. After centrifugation, the supernatant was transferred into a new tube and incubated overnight at 65°C to reverse the crosslink. 750  $\mu$ L of Trizol and 200  $\mu$ L of Chloroform was added to each sample and the aqueous phase was collected. RNA was precipitated overnight at  $-20^{\circ}$ C by addition of 500  $\mu$ L of propanol and 1  $\mu$ L of glycogen. After centrifugation, RNA pellet was washed in 70% ethanol and resuspended in 30  $\mu$ L of bi-distilled water for IP samples and 20  $\mu$ L of water for Input samples. Total mRNAs were then reverse-transcribed and amplified by quantitative PCR.

### Polysome profiling

**Cell lysis.**  $2 \times 10^9$  cells were used for each polysome profiling experiment. 100  $\mu$ g/ml of cycloheximide was added for 5 minutes to each sample to “freeze” ribosomes onto RNAs. Cells were centrifuged, washed two times with 7 mL of pre-lysis buffer (20mM Tris-HCl pH8, 50mM KCl, 10mM MgCl<sub>2</sub>, 1mM DTT, 100 $\mu$ g/mL cycloheximide, 200  $\mu$ g/mL heparin) and then resuspended in a volume of lysis buffer (20mM Tris-HCl pH8, 50mM KCl, 10mM MgCl<sub>2</sub>, 1mM DTT, 100 $\mu$ g/mL cycloheximide, 200 $\mu$ g/mL heparin, Ultra-protease inhibitor 1X-Roche, and 40U/ml RNasin-Promega) equivalent to the cell pellet size. An equal volume of zirconium beads was added to the cell suspension and cells were mechanically lysed thanks to use of a bead-beater. Lysate was recovered and cleared by centrifugation.

**Polysomal profiles.** 15 and 50% sucrose buffers were prepared in 50mM NH<sub>4</sub>Cl, 50mM Tris-Acetate, 12mM MgCl<sub>2</sub>, 1mM DTT. To obtain a linear gradient, we used the Gradient Maker device (Hoefer SG) equipped with tubes adapted for a SW41 rotor. We used 11ml of each sucrose buffer in each gradient tube. Cytoplasmic extracts with equal amounts of RNA were loaded on the 15%–50% sucrose gradient and centrifuged at 4°C in a SW41Ti Beckman rotor for 3h30 min at 39,000 rpm. Absorbance at 254 nm was recorded by BioLogic LP software (Bio-Rad) and fractions (0.5 ml each) were collected for subsequent RNA extraction.

To distinguish between active polysomes and co-sedimenting mRNPs, we treated our samples with 40 mM EDTA prior to gradient loading. Sucrose gradients were also supplemented with 30 mM EDTA and prepared without Mg<sup>2+</sup>.

**RNA purification.** The different fractions were pooled into 3 major fractions: cytoplasm, monosomes and polysomes. 100  $\mu$ g/ml of proteinase K and 1% SDS was added to each major fraction. The fractions were then incubated for 1h30 at 37°C. 200mM NaCl and 1/4 volume of acidic phenol/chloroform/isoamyl alcohol (25:24:1) was added to the samples and the aqueous phase was transferred to a new tube. RNAs were precipitated overnight at  $-20^{\circ}$ C after addition of 1  $\mu$ L of glycogen and 1 volume of isopropanol. After centrifugation, RNA pellet was washed in 70% ethanol and resuspended in 120  $\mu$ L of bi-distilled water. mRNAs were then re-purified using the RNeasy mini kit (QIAGEN) and eluted in 80  $\mu$ L of the elution buffer of the kit. RNAs were again precipitated overnight at  $-20^{\circ}$ C after addition of 40 mM Na-acetate, 1  $\mu$ L of glycogen and 212  $\mu$ L of ethanol 100%. After centrifugation, RNA pellet was washed in 70% ethanol and resuspended in 40  $\mu$ L of bi-distilled water. The RNA concentration was measured using nanodrop. mRNAs were then reverse-transcribed and amplified by quantitative PCR.

### Quantification and statistical analysis

Number of replicates and statistical tests are specified in the corresponding figure legends. In all graphs, standard deviations are represented by error bars. Western blots were quantified using the Image lab software (Biorad). Raw files (.scn) were used to allow the quantification of linear and non-saturated signals. 2D gels were quantified using the Image Quant software (GE Healthcare). The mass spectrometry analysis is described in the corresponding paragraph of the [STAR Methods](#).

### Data and software availability

Proteomic data as raw files, total proteins and peptides identified with relative intensities and search parameters have been loaded on the Peptide Atlas repository (<http://www.peptideatlas.org/PASS/PASS01156>). The remaining raw data have been deposited to Men-deley Data and are available at <http://dx.doi.org/10.17632/wwrcg942cf.1>.